

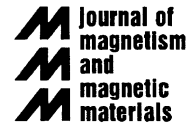


ELSEVIER

Available online at www.sciencedirect.com

SCIENCE @ DIRECT®

Journal of Magnetism and Magnetic Materials 301 (2006) 389–397



www.elsevier.com/locate/jmmm

Roles of spin-polarized current and spin accumulation in the current-induced magnetization switching

T. Yang^{a,b,*}, J. Hamrle^{a,b}, T. Kimura^{a,b,c}, Y. Otani^{a,b,c}

^aQuantum Nano-scale Magnetics Laboratory, Frontier Research System, RIKEN, 2-1 Hirosawa, Wako, Saitama 351-0198, Japan

^bCREST, Japan Science & Technology Corporation, Japan

^cInstitute of Solid State Physics, University of Tokyo, Kashiwa, Chiba 227-8581, Japan

Received 20 June 2005; received in revised form 23 July 2005

Available online 15 August 2005

Abstract

To clarify the contributions of spin-polarized current and spin accumulation to the current-induced magnetization switching, the effects of the top electrode size of the magnetic nanopillar are investigated both theoretically and experimentally. Theoretical calculation demonstrates that the spin-polarized current and the spin accumulation can be adjusted in opposite directions by modifying the size of the top electrode. Increase in the size of the top electrode suppresses the spin accumulation but enhances the spin-polarized current inside the nanopillar. On the other hand, it is shown experimentally that the nanopillar with a wide top electrode exhibits small critical switching current compared to the nanopillar with a narrow top electrode. The results suggest that the spin-polarized current contributes to the current-induced magnetization switching dominantly over the spin accumulation.

© 2005 Elsevier B.V. All rights reserved.

PACS: 72.25.Ba; 85.75.Bb; 73.63.Rt

Keywords: Spin-polarized current; Spin accumulation; Spin-transfer; Nanopillar; CPP-GMR

1. Introduction

Traditionally, a magnetic field is necessary to reverse the magnetization of a magnet. However, it

is found recently that a DC current passing through a nanoscale magnet can also switch the magnetization. This was theoretically predicted by Slonczewski [1] and Berger [2] in 1996. The first experimentally realization by Katine et al. [3] has stimulated extensive studies [4–15] on the current-induced magnetization switching (CIMS).

To realize the CIMS, the DC current must be spin-polarized. Therefore, most of the studies on

*Corresponding author. Quantum Nano-scale Magnetics Laboratory, Frontier Research System, Riken, 2-1 Hirosawa, Wako, Saitama 351-0198, Japan. Tel.: +81 48 462 1111; fax: +81 48 467 9650.

E-mail address: tyang@riken.jp (T. Yang).

CIMS are carried out with a nanoscale current-perpendicular-to-the-plane giant magnetoresistance (CPP-GMR) device, also known as the nanopillar. The nanopillar comprises two magnetic layers separated by a nonmagnetic layer. One of the two magnetic layers takes the role of spin polarizer with fixed magnetization while the other one is a free layer with reversible magnetization. Because of its two stable collinear configurations of the magnetizations of the two magnetic layers, i.e. antiparallel (AP) and parallel (P) configurations, the CPP-GMR nanopillar device is promising for the application to the magnetic random access memory (MRAM). The realization of CIMS would simplify the MRAM device structure and therefore improve the storage density.

When a DC charge current I_{ch} passes through the nanopillar device, two physical processes occur. Firstly, the spins of the conductive electrons take only two directions, parallel or antiparallel to the local magnetization. Accordingly, the electrical current is divided into two parts, spin-up electrical current I_{\uparrow} and spin-down electrical current I_{\downarrow} . Because of the spin-dependent scattering inside the magnetic layers, the spin-up current is larger than the spin-down current. Thus, the DC current is spin-polarized in the device. The difference between the two currents is the spin-polarized current $I_{\text{sp}} = I_{\uparrow} - I_{\downarrow}$. On the other hand, when the spin-polarized current passing through the device, spin surplus appears in both the magnetic and nonmagnetic layers, known as the spin accumulation. The spin accumulation is expressed as the splitting of the electrochemical potential $\Delta\mu = \mu_{\uparrow} - \mu_{\downarrow}$.

The CIMS has been explained with either the spin-polarized current or the spin accumulation. Theories based on the former believe that the spin-polarized current transfers the transverse component of the spin angular momentum to the local magnetic moment at the interface upon flowing into the free magnetic layer [1,9–11], when there is a small deviation from the collinear configuration of the magnetizations. Thereby a torque is exerted on the local moment, resulting in the spin-wave excitation or the magnetic switching. However, the theory of nonequilibrium exchange interaction (NEXI) [8] claims that the effective field due to

the spin accumulation should contribute to the CIMS. There are also theories [12–14] suggesting that the spin accumulation results in a transverse spin current at the interface responsible for the CIMS. Nevertheless, the roles of the spin-polarized current and the spin accumulation in the CIMS have not been clarified yet.

As the simplest one-dimensional (1D) case, the spin-polarized current is correlated with the spin accumulation as in following diffusion equations [16]

$$j_{\uparrow,\downarrow} = \frac{\sigma_{\uparrow,\downarrow}}{e} \frac{\partial \mu_{\uparrow,\downarrow}}{\partial x} \quad (1)$$

and

$$\frac{\Delta\mu}{\lambda^2} = \frac{\partial^2 \Delta\mu}{\partial x^2}, \quad (2)$$

where λ , μ , σ and e are, respectively, the spin-diffusion length, the electro-chemical potential, the electrical conductivity, and the electronic charge. From the above equations, at least in the nonmagnetic layer, where $\sigma_{\downarrow} = \sigma_{\uparrow}$, the spin-polarized current depends on the gradient of $\Delta\mu$. Therefore the spin accumulation and the spin-polarized current are not necessarily increased or decreased simultaneously. Thus, it is important to clarify their roles for not only further understanding the physical mechanism but also the practical application. However, corresponding experimental studies are still absent up to now.

In this paper, it will be shown theoretically that the spin-polarized current and the spin accumulation inside the nanopillar can be adjusted in opposite directions through modifying the size of the top electrode. In this way, the dominant contribution to the CIMS can be experimentally determined by studying the switching behaviors.

2. Theoretical calculation

To obtain the spatial distribution of the spin-polarized currents and the spin accumulation in a nanopillar device, which is difficult to be measured experimentally, we have proposed a formalism expressing such a structure as a 3D circuit of spin-dependent resistor elements (3D-SDRE), wherein the propagation is regarded as a 1D problem [17].

To our knowledge, it is the first time that a 3D calculation of the spin-polarized current is carried out.

With this formalism, we studied how the size of the top electrode influences the spin-polarized current and the spin accumulation in the nanopillar with a layered structure of Cu1/Co1 (40 nm)/Cu2 (6 nm)/Co2 (2 nm)/Cu3, wherein Cu1 and Cu3 take the roles of bottom and top electrodes, respectively. The pillar shape is square with the size of 100 nm. The considered structure types are shown in Fig. 1. The top electrode Cu3 in (a) (A-structure) is horizontally extended while in (b) (B-structure) is standing on the pillar and has the same cross-sectional area with the pillar. The extended homogeneous layers Cu1 and Cu3 in (a) and Cu1 in (b) are approximated as a square pillar of 800 nm in size. The magnetization of the Co1 layer is always fixed as “up” (\uparrow), whereas the magnetic orientations of the Co2 layer is varied. The charge current perpendicularly passing through the structure is assumed to be $I_{\text{ch}} = 1$ mA, equivalent to the average charge current density in the pillar $j_{\text{ch}} = 1 \times 10^7$ A/cm². The electrical properties of materials are of room temperature: electric conductivity $\sigma_{\text{Cu}} = 48.1 \times 10^6 \Omega^{-1} \text{m}^{-1}$, $\sigma_{\text{Co}} = 4.2 \times 10^6 \Omega^{-1} \text{m}^{-1}$, spin-flip lengths $\lambda_{\text{Cu}} = 350$ nm, $\lambda_{\text{Co}} = 60$ nm, and Co spin bulk asymmetry $\gamma = 0.35$. We assume no interface resistance, and no interface or surface scattering. The largest SDRE grid size is 10 nm.

Fig. 2(a) shows the calculated profile of the spin-polarized current density j_{sp} along the central axis of the structures in Fig. 1. In both the A-structure and the B-structure, j_{sp} for the parallel Co1 and Co2 layers ($\uparrow\uparrow$) is larger than that for the antiparallel configuration ($\uparrow\downarrow$). Furthermore, j_{sp} is enhanced inside the nanopillar for the A-structure compared to the B-structure. Averaging over the whole pillar cross-sectional area yields j_{sp} values at Co2 layer of 29.4×10^5 A/cm² for the A-structure and 19.0×10^5 A/cm² for the B-structure.

The origin of the j_{sp} enhancement in the A-structure is as follows: the pillar with the A-structure is attached to an infinitely large Cu layer (Cu3), which acts as a reservoir, with $\Delta\mu = \mu_{\uparrow} - \mu_{\downarrow} = 0$. In other words, the infinitely

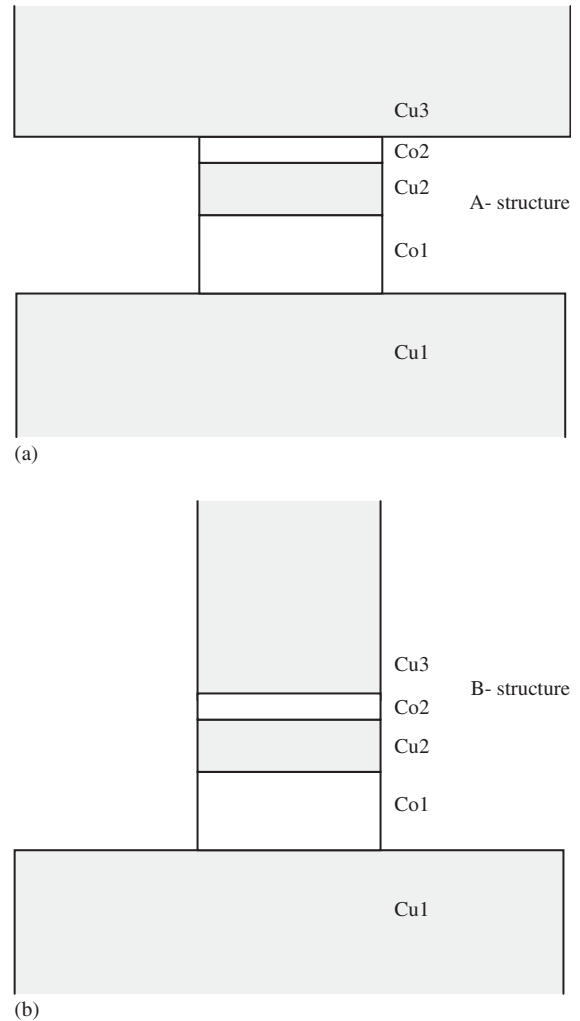


Fig. 1. Sketches of the studied structure types. (a) Nanopillar with horizontally extended top electrode, and (b) nanopillar with top electrode having the same cross-sectional area as the nanopillar.

large Cu3 layer provides a large volume for the spin-polarized current to be scattered, thus acting as a strong spin-flip scatterer. Hence, the infinitely large Cu3 layer works as a small shortcircuiting resistance between up and down channels. Consequently, shortcircuiting of up and down channels leads to an increase in j_{sp} .

Presented in Fig. 2(b) are the profiles of μ_{\uparrow} and μ_{\downarrow} along the central axis of both structures. Only parallel configurations are presented here. In

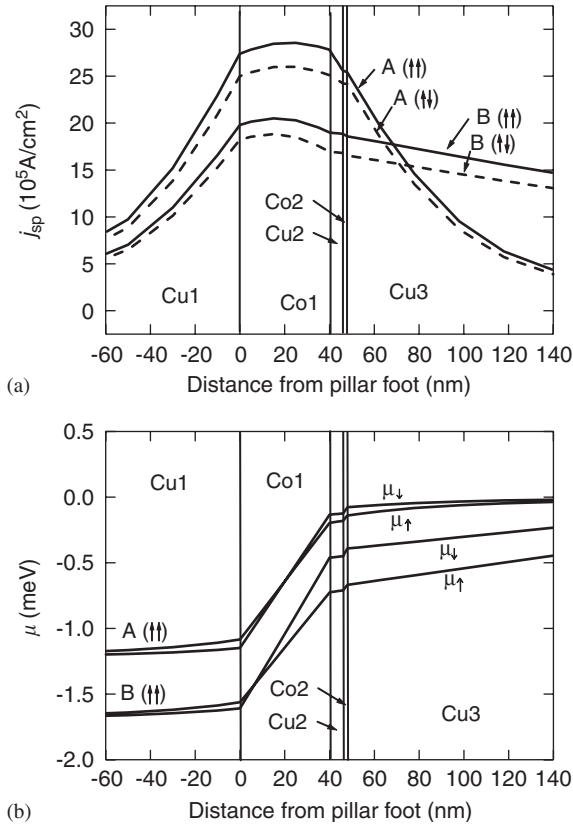


Fig. 2. Calculated profiles of (a) the spin-polarized currents and (b) the chemical potentials along the central axis of the two kinds of structures.

contrast to j_{sp} , Fig. 2(b) exhibits a suppression of $\Delta\mu$ in the A-structure not only in the Cu3 layer but also inside the nanopillar. The reason is exactly the same as discussed above: the infinitely large Cu3 layer works as a strong spin scatterer, causing a small spin-flip resistance (large scattering) between up and down channels. Obviously, such a shortcut reduces $\Delta\mu$. The $\Delta\mu$ at Co2 layer averaged over the whole pillar cross-sectional area is -0.267 meV for the B-structure and -0.052 eV for the A-structure. Berger [13] has also pointed out the suppression of $\Delta\mu$ in a large top electrode in his calculation.

The above calculation shows that the top electrode outside the nanopillar can influence the spin-polarized current and the spin accumulation inside the nanopillar. It is further demonstrated that the spin-polarized current and the spin

accumulation can be adjusted in opposite directions with changing the size of the top electrode. This provides the possibility to experimentally study their respective roles in the CIMS.

3. Experimental results and discussion

Based on the theoretical conclusions, we have fabricated two groups of nanopillars with different top electrode size, and studied their CIMS behaviors.

The fabrication process is the combination of electron-beam evaporation, photolithography, ion milling, magnetron sputtering, and electron beam lithography [18]. The studied nanopillars comprise a layered structure of Cu1 (60 nm)/Co1 (40 nm)/Cu2 (6 nm)/Co2 (2.5 nm)/Au (20 nm)/Cu3 (50 nm). The layers of Cu1 (60 nm) and Cu3 (50 nm) serve as the bottom and the top electrodes, respectively. The bottom Co1 (40 nm) layer is extended to avoid the dipolar coupling between the two Co layers. It has a fixed magnetization during the current-induced magnetization switching, while the top Co2 (2.5 nm) layer has freely switchable magnetization. During the fabrication, Cu1 (60 nm)/Co1 (40 nm)/Cu2 (6 nm)/Co2 (2.5 nm)/Au (20 nm) multilayers are firstly deposited with electron-beam evaporation while the 50 nm top electrode is finally evaporated after the formation of the nanopillar. The 20 nm Au layer is deposited to prevent oxidation during the fabrication.

Corresponding to Fig. 1(a), one group of the nanopillars have top electrodes as wide as $9 \mu\text{m}$. In comparison, the top electrodes for the nanopillars in the other group are as narrow as $\sim 100 \text{ nm}$, representing the case of Fig. 1(b). As a realistic structure, the narrow top electrode lies on the nanopillar horizontally, unlike the standing one shown in Fig. 1(b).

However, it is technically difficult to align a top electrode of $\sim 100 \text{ nm}$ in width onto a nanopillar of $\sim 100 \text{ nm}$. To solve this problem, a grid-shaped top electrode illustrated in Fig. 3(a) is designed. The slits of the grid are narrower than the nanopillar whereas the width of the conductive strips between the slits is comparable to the nanopillar. There are tens of strips in one grid so that the probability of

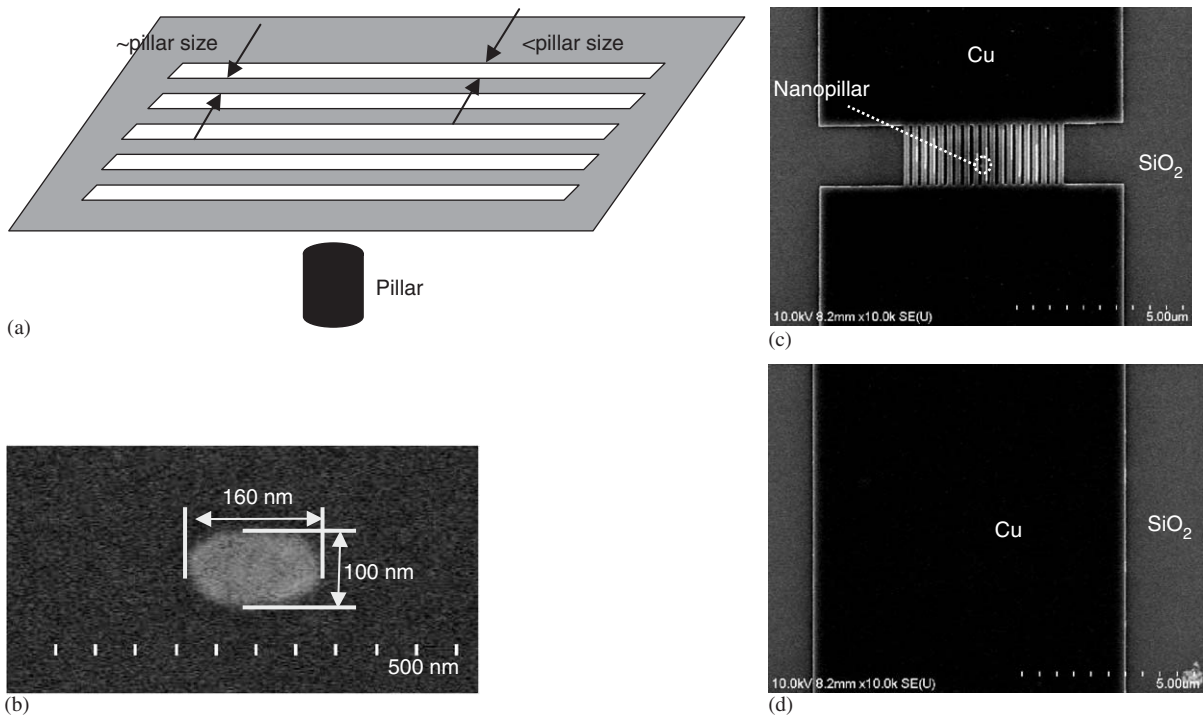


Fig. 3. (a) Schematics of the grid-shaped top electrode, and SEM images of (b) a nanopillar (top view), (c) the grid-shaped Cu electrode, as well as (d) the wide Cu electrode.

the nanopillar being covered by one strip is effectively increased. The length of the conductive strips is designed to be much larger than the spin-diffusion length. Therefore the strip is equivalent to the narrow top electrode.

Since the Au surface of the nanopillar is exposed to the resist and chemicals during the processing, it is cleaned with ion milling prior to the top Cu electrode deposition. This ion milling removes more than 5 nm Au. Then the sample is quickly moved from the ion-milling chamber into the evaporation chamber so that the Au/Cu interface is remained as clean as possible. In addition, the remained Au is less than 15 nm, well below the spin-diffusion length of the evaporated Au at room temperature. The spin-diffusion length of the sputtered Au has been measured to be 63 nm [19] at 10 K or 150 nm [20] at 4.2 K. These values are reduced to roughly one-third at room temperature but doubled for evaporated Au [20]. Thus the evaporated Au has a spin-diffusion length of

about 42 or 100 nm at room temperature. Therefore, most of the polarization of the current is remained after passing the Au layer.

Fig. 3(b) shows the top-view scanning electron microscope (SEM) image of the fabricated nanopillar with the size of $160 \times 100 \text{ nm}^2$. Figs. 3(c) and (d) are the SEM images of a grid-shaped narrow Cu electrode and a wide Cu electrode, respectively. The white circle in (c) indicates the position of the nanopillar, roughly being the middle of the strip length. Because of the misalignment, some nanopillars are fully covered with a single Cu strip while the others are only partially covered.

The perpendicular transport properties of the pillars are measured by means of lock-in technique at room temperature. To compensate the possible dipolar-coupling field between the two Co layers, the differential resistance (dV/dI) vs. DC current (I_{DC}) loops are measured with varying the applied field along the long axis of the elliptic pillar. Since both the external field and the dipolar-coupling

field cause shift and shrinkage of the dV/dI vs. I_{DC} loop [21], the averaged critical switching current is determined from the widest loop in the measurement. The widest loops are always obtained with zero or small external fields because of the small dipolar coupling in our samples.

It is found that only the nanopillars fully covered with the top electrode exhibit sharp single-step magnetic switching with both magnetic field and DC current. This suggests that the contact area between the top electrode and the nanopillar possibly affects the switching behavior. We do not study this possibility in this paper. The results reported hereafter are for the fully covered nanopillars.

Figs. 4(a) and (b) are the MR loops for two nanopillars with the wide and the grid-shaped narrow top electrodes, respectively. The two peaks are well separated, implying a small dipolar coupling between the two Co layers. The corresponding dV/dI vs. I_{DC} loops are plotted in Figs. 4(c) and (d). For both nanopillars, either the applied field or the DC current induces sharp and full transitions between the AP and P states. The nanopillar with the wide top electrode has a reasonable resistance of about 1.1Ω and a MR ratio of 4.2%. However, the resistance of the nanopillar with the grid-shaped electrode is as high as 3.0Ω . This high value is caused by the

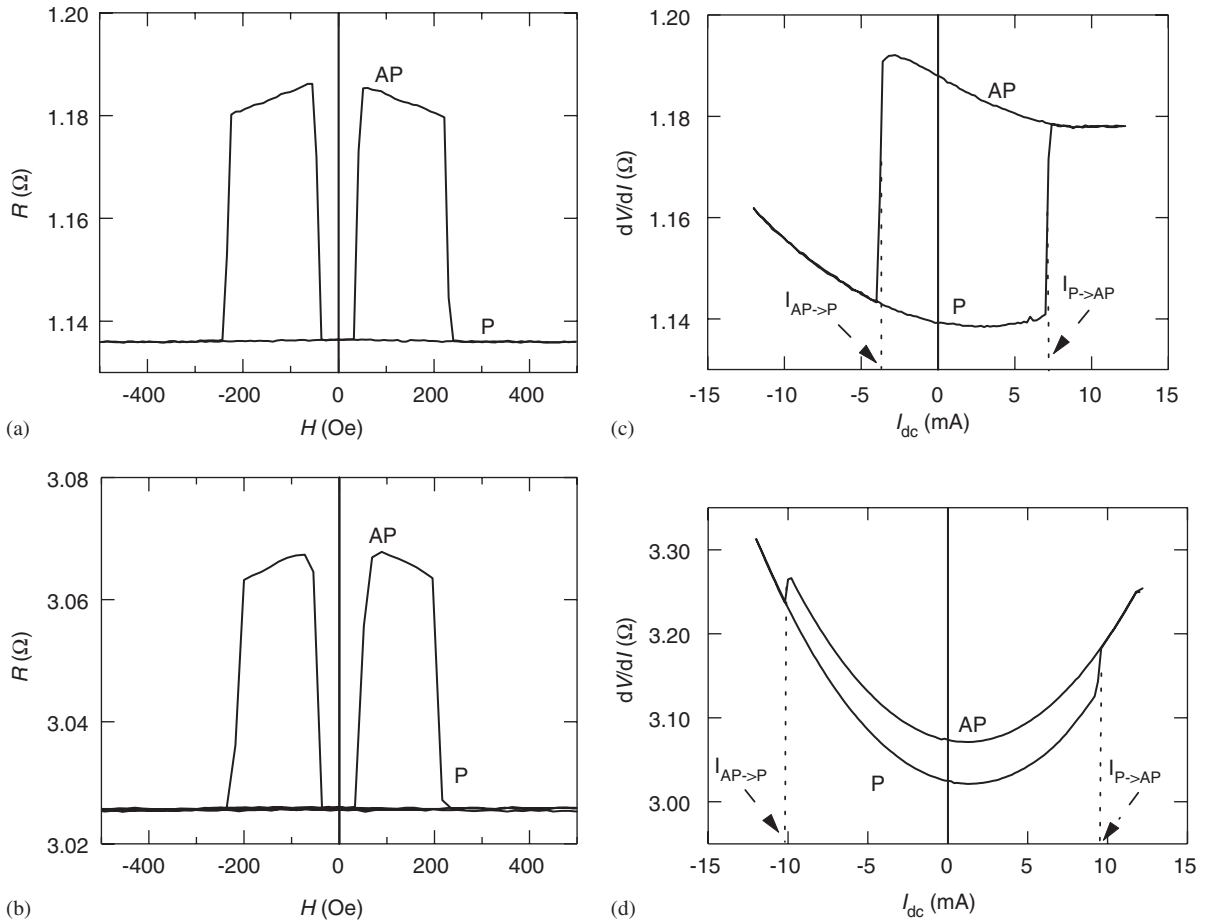


Fig. 4. MR loops for nanopillars with (a) the wide top electrode, and (b) the grid-shaped narrow top electrode. dV/dI vs. I_{DC} loops for nanopillars with (c) the wide top electrode, and (d) the grid-shaped top narrow electrode.

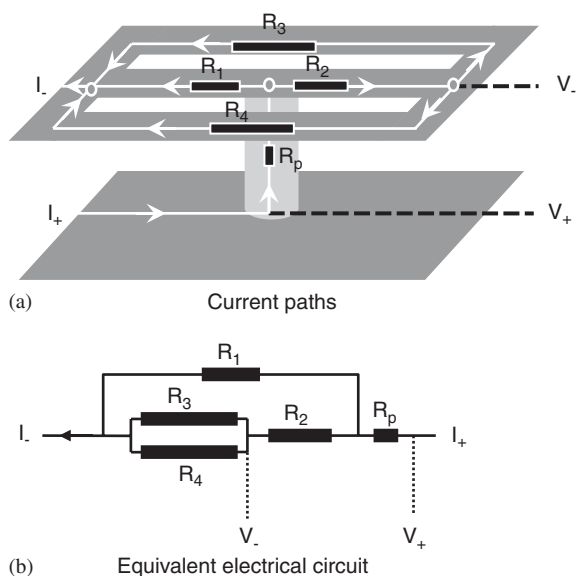


Fig. 5. (a) Current paths in the nanopillar and the grid-shaped top electrode, and (b) the equivalent electrical circuit. R_{1-4} are the resistances in the strips while R_p is the resistance of the nanopillar.

grid-shaped electrode, in which the electrical current flows along the paths shown in Fig. 5(a). It can be understood from the equivalent circuit in Fig. 5(b) that the measured resistance includes the contribution of the top electrode as well as the pillar resistance. Therefore the measured resistance is much higher than that of the nanopillar itself. The two samples are fabricated from the same chip and have the same size of $160 \times 100 \text{ nm}^2$. The only difference between them is the top electrode.

Remarkable is a large difference in the critical switching current seen as a change in width of the two dV/dI vs. I_{DC} loops in Figs. 4(c) and (d). The critical switching current density is determined from half of the loop width and the cross-sectional area of the nanopillar, being $4.2 \times 10^7 \text{ A/cm}^2$ for the wide top electrode and $7.8 \times 10^7 \text{ A/cm}^2$ for the grid-shaped narrow top electrode. The latter is 1.8 times as large as the former. Listed in Table 1 are the critical switching currents for the nanopillars with the size of $160 \times 100 \text{ nm}^2$. In average, the critical switching current is increased by a factor of 1.8 when the wide top electrode is replaced with the narrow one. The increase of the critical

Table 1

Comparison of the critical switching current between nanopillars with the narrow top electrode (3 samples) and the wide top electrode (3 samples) respectively. The size of the pillars is $160 \times 100 \text{ nm}^2$

Sample No.	Critical switching current (mA)	
	Narrow top electrode	Wide top electrode
#1	8.0	4.3
#2	9.3	5.4
#3	9.9	5.6

switching current is also observed with the nanopillars with the size of $130 \times 70 \text{ nm}^2$, for which the factor of increase is 1.6 in average.

One possible reason for the difference in the critical switching current is the Oersted field due to the current flowing in the narrow top electrode. According to the magnetization direction of the bottom Co layer, this Oersted field should cause expansion or shrinkage of the dV/dI vs. I_{DC} loop. To examine the influence of this Oersted field, the magnetization of the bottom Co is reversed, and then the dV/dI vs. I_{DC} loop is measured again. Almost the same result is obtained, meaning that the influence of the current in the top electrode is negligible. In fact, because of the symmetric structure of the grid-shaped electrode, the Oersted fields from the strips are nearly cancelled.

According to our theoretical calculation, increase in the size of the top electrode diminishes the spin accumulation at the Co2 layer by a factor up to 5. In Berger's calculation [13], this factor is 2. Our calculation also shows that the spin-polarized current at the Co2 layer is increased by a factor of about 2. This is because that the wide electrode provides a large volume for conduction-electron-spin relaxation, thus acting as a strong spin-flip scatterer. Hence, the wide top Cu electrode works as a small shortcutting resistance between up and down channels. Consequently, shortcutting of up and down channels leads to an increase in the spin-polarized current and the suppressing of the spin accumulation even inside the nanopillar. This can also be explained by employing the spin resistance $R_S = \lambda/[\sigma A(1 - \alpha^2)]$, where A is the cross-sectional area, and α is the spin asymmetry. Increase in the

area A decreases the value of R_S , and thus accelerates the spin-flip scattering.

The theoretical and experimental results can be summarized as follows. By increasing the size of the top electrode, inside the nanopillar the spin-polarized current is increased while the spin accumulation is decreased. At the same time the critical switching current for the CIMS is also decreased. In other words, the switching is facilitated. Thus, it could be concluded that the spin-polarized current is the dominant contribution to the CIMS. The increase of the spin-polarized current equals to the increase of the polarization of the charge current $p = I_{sp}/I_{ch}$. Since the critical spin-polarized current I_{sp} for the CIMS does not change, the increase of p reduces the critical switching current I_{ch} .

In contrary to the present conclusion, previous theoretical works [12–14] suggested that the spin accumulation is responsible for the CIMS. These previous conclusions support the strategy that the spin accumulation should be increased to reduce the critical current for magnetic switching. However, the present results show that the large spin accumulation in the nanopillar with the narrow top electrode does not correspond to a small switching current, whereas the increase in the spin-polarized current reduces the critical switching current. Thus, it is clear that the spin-polarized current is the dominant contribution to the CIMS. With the present results, we do not deny the contribution of the spin accumulation, but show that it is much ineffective compared to the contribution of the spin-polarized current. Therefore, to reduce the critical switching current, the polarization of the charge current should be increased. The possible ways are to introduce spin-flip scatterers in the electrode or to use capping layers with short spin-diffusion length.

Finally, we briefly discuss the influence of the spin pumping effect [22]. Since the CIMS is realized through the precession of the magnetization, the spin pumping effect possibly occurs, increasing the damping coefficient and accordingly the critical switching current. Because the spin pumping effect also depends on the adjacent nonmagnetic layer, one may argue that the change of the switching current is caused by the spin

pumping other than the spin-polarized current as we claim in this paper. However, it should be noticed that the spin accumulation build-up in the nonmagnetic layer opposes the spin pumping. Therefore, the spin pumping should be weaker for the narrow top electrode than for the wide top electrode. Nevertheless, the critical switching current is increased in the narrow top electrode compared to the wide top electrode. Hence, the change of the critical switching current is unlikely caused by the spin pumping.

4. Conclusions

Theoretical calculation demonstrates that the spin-polarized current and the spin accumulation inside the nanopillar can be adjusted in opposite directions through modifying the size of the top electrode. The expansion of the top electrode increases the spin-polarized current, but reduces the spin accumulation. Corresponding experimental study further reveals that the expansion of the top electrode also reduces the critical switching current, facilitating the magnetization switching. Therefore it could be concluded that the spin-polarized current makes the dominant contribution to the current-induced magnetic switching in the CPP-GMR device.

Acknowledgements

We are grateful to Dr. Tsukagoshi and the Nanoscience Development and Support Team of RIKEN for their kind supports.

References

- [1] J.C. Slonczewski, *J. Magn. Magn. Mater.* 159 (1996) L1.
- [2] L. Berger, *Phys. Rev. B* 54 (1996) 9353.
- [3] J.A. Katine, F.J. Albert, R.A. Buhrman, E.B. Myers, D.C. Ralph, *Phys. Rev. Lett.* 84 (2000) 3149.
- [4] J. Grollier, V. Cros, A. Hamzic, J.M. George, H. Jaffre's, A. Fert, G. Faini, J. Ben Youssef, H. Legall, *Appl. Phys. Lett.* 78 (2001) 3663.
- [5] J.Z. Sun, D.J. Monsma, D.W. Abraham, M.J. Rooks, R.H. Koch, *Appl. Phys. Lett.* 81 (2002) 2202.
- [6] S. Urazhdin, N.O. Birge, W.P. Pratt Jr., J. Bass, *Phys. Rev. Lett.* 91 (2003) 146803.

- [7] S.I. Kiselev, J.C. Sankey, I.N. Krivorotov, N.C. Emley, R.J. Schoelkopf, R.A. Buhrman, D.C. Ralph, *Nature* 425 (2003) 380.
- [8] C. Heide, P.E. Zilberman, R.J. Elliott, *Phys. Rev. B* 63 (2001) 064424.
- [9] M.D. Stiles, A. Zangwill, *J. Appl. Phys.* 91 (2002) 6912.
- [10] X. Waintal, E.B. Myers, P.W. Brouwer, D.C. Ralph, *Phys. Rev. B* 62 (2000) 12317.
- [11] A.A. Kovalev, A. Brataas, G.E.W. Bauer, *Phys. Rev. B* 66 (2002) 224424.
- [12] L. Berger, *J. Appl. Phys.* 89 (2001) 5521.
- [13] L. Berger, *J. Magn. Magn. Mater.* 278 (2004) 185.
- [14] A. Fert, V. Cros, J.-M. George, J. Grollier, H. Jaffrès, A. Hamzic, A. Vaurès, G. Faini, J. Ben Youssef, H. Le Gall, *J. Magn. Magn. Mater.* 272–276 (2004) 1706.
- [15] J. Zhang, P.M. Levy, S. Zhang, *Phys. Rev. Lett.* 93 (2004) 256602.
- [16] P.C. van Son, H. van Kempen, P. Wyder, *Phys. Rev. Lett.* 58 (1987) 2271.
- [17] J. Hamrle, T. Kimura, T. Yang, Y. Otani, *Phys. Rev. B* 71 (2005) 094434.
- [18] T. Yang, T. Kimura, Y. Otani, *J. Appl. Phys.* 97 (2005) 064304.
- [19] Y. Ji, A. Hoffmann, J.S. Jiang, S.D. Bader, *Appl. Phys. Lett.* 85 (2004) 6218.
- [20] Wen-C. Chiang, C. Ritz, K. Eid, R. Loloee, W.P. Pratt Jr., J. Bass, *Phys. Rev. B* 69 (2004) 184405.
- [21] S. Urazhdin, H. Kurt, W.P. Pratt Jr., J. Bass, *Appl. Phys. Lett.* 83 (2003) 114.
- [22] Y. Tserkovnyak, A. Brataas, *Phys. Rev. B* 66 (2002) 224403.